Near-weld creep crack growth behaviour in Type 316H steel ex-service components

Haoliang Zhou[1], Ali Mehmanparast[2*], Kamran Nikbin[1]

[1]Department of Mechanical Engineering, Imperial College London, South Kensington Campus, London, SW7 2AZ, UK

[2]Offshore Renewable Energy Engineering Centre, Cranfield University, Cranfield, Bedfordshire, MK43 0AL, UK

*Corresponding author: a.mehmanparast@cranfield.ac.uk

Abstract:

Creep crack growth is known to be the dominant failure mechanism in high temperature components. Particularly in welded structures operating at elevated temperatures, cracks are often found to initiate and propagate in the vicinity of the weld region which can eventually penetrate into the base material after a long period of operation. In this study, creep crack growth tests have been performed on specimens extracted from an ex-service 316H welded component to examine the crack initiation and growth behaviour in near-weld regions. The results show that the cracking behaviour of the base metal in near-weld specimens is similar to the as-received 316H data set, suggesting that the material inhomogeneity would not influence the crack propagation behaviour in service exposed components. Moreover, the test results show that the crack initiation and growth behaviour of the HAZ specimens can be estimated in much shorter time scales by performing tests on pre-compressed material.

Keywords: Creep; Creep crack growth; 316H; CCG; NSW; C* correlation, Weld

Nomenclature:

a	Crack length
a_0	Initial crack length
$\dot{a}$	Crack extension rate
$\dot{a}_{NSW}$	Creep crack growth rate predicted by NSW model
$\dot{a}_{NSWA}$	Creep crack growth rate predicted by NSWA model
$\dot{a}_{NSW-MOD}$	Creep crack growth rate predicted by NSW-MOD model
Δa	Crack extension
A	Norton power-law constant
A_s	Creep stress coefficient in steady state creep strain law
A_A	Creep stress coefficient in average creep strain law
B	Specimen thickness
B_n	Net thickness between the side grooves
B_r	Stress coefficient in creep rupture law

This is a peer-reviewed, accepted author manuscript of the following article: Zhou, H., Mehmanparast, A., & Nikbin, K. (2020). Near-weld creep crack growth behaviour in type 316H steel ex-service components. Materials at High Temperatures , 37(6), 488-498. https://doi.org/10.1080/09603409.2020.1831143

C^*	Steady state creep fracture mechanics parameter
D	Material constant in creep crack growth correlation with C^*
E	Elastic Young's modulus
E'	Effective Young's modulus
$\bar{h}_n$	Maximum of $\tilde{\bar{\varepsilon}}(\theta,n)/\varepsilon_f^*(\theta,n)$ in NSW-MOD model
H	Non-dimensional function of specimen geometry and n
I_n	A dimensionless integration constant
n	Creep stress exponent
n_A	Creep stress exponent in average creep strain law
K	Stress intensity factor
P	Applied load
t	Time
$t_{0.2}$	Time for 0.2 mm crack extension
$t_{0.5}$	Time for 0.5 mm crack extension
t_i	Initiation time
t_f	Test duration
t_T	Transition time
t_r	Time to rupture
r_c	Creep process zone size
W	Specimen width
σ	Applied stresses
σ_0	Normalising stress
σ_{ref}	Reference stress
$\dot{\varepsilon}_0$	Normalising strain rate
$\dot{\varepsilon}_s^c$	Steady state creep strain rate
$\dot{\varepsilon}_A^c$	Average creep strain rate
ε_f	Uniaxial creep ductility
ε_f^*	Multiaxial creep ductility
$\tilde{\bar{\varepsilon}}$	Equivalent strain as a function of θ and n in NSW-MOD model
Δ	Load line displacement
$\dot{\Delta}$	Load line displacement rate
$\dot{\Delta}^C$	Component of displacement rate associated with the accumulation of creep strains
$\dot{\Delta}^T$	Total load line displacement rate
Δ^{LLD}	Load line displacement
ϕ	Material constant in creep crack growth correlation with C^*

λ	Non-dimensional crack velocity
η	Factor relating C^* to load and displacement measurements
θ	Crack tip angle
ν_r	Temperature dependent constant in creep rupture law
ν	Poisson's ratio
AGR	Advanced Gas-cooled Reactor
AR	As-Received material
BM	Base Metal
C(T)	Compact Tension specimen
CCI	Creep Crack Initiation
CCG	Creep Crack Growth
DCPD	Direct Current Potential Drop
EDM	Electrical Discharge Machining
HAZ	Heat Affected Zone
LLD	Load Line Displacement
LVDT	Linear Variable Differential Transformer
MMA	Manual Metal Arc
NSW	Nikbin, Smith and Webster creep crack growth model
NSWA	Approximate NSW model
NSW-MOD	Modified version of the NSW model
PC	Pre-Compressed material
ROA	Reduction Of Area
SEN(T)	Single Edge Notched specimen in Tension
SS	Stainless Steel
XW	Cross-Weld

1. Introduction

Type 316H stainless steel (SS) is widely used in the UK Advanced Gas-cooled Reactor (AGR) power plant components. These components operate at elevated temperatures with creep damage identified as the dominant failure mechanism [1]. As a consequence of operation at elevated temperatures, reheat cracking has been repeatedly found in the heat affected zone (HAZ) of the thick-walled steam header welded components [2][3]. This has been attributed to the creep deformation and damage driven by highly triaxial residual stresses [4][5]. An important issue to be understood in the life assessment of AGR power plant steam header components is therefore the crack initiation and crack growth behaviour in near-weld regions due to reheat cracking. Steam headers which have operated for a long period of time at high temperatures are prone to reheat cracking in the vicinity of the weld region which is evident to be driven by the welding residual stresses [6]. By quantifying the residual stress distribution in the weld sections, it has been shown in previous studies that the weld-induced residual stresses

could significantly influence the creep crack initiation (CCI) and early stage creep crack growth (CCG) behaviour of the material [7]-[11]. Furthermore, it has been shown by other researchers than the CCI and CCG behaviour in high temperatures components is influenced by material aging due to service exposure and inhomogeneity in the HAZ and weld regions [12][13].

In order to fill in the knowledge gap, the present study aims to facilitate the evaluation of the remaining life in 316H welded steam header components by performing CCG tests on near-weld specimens. For this purpose, CCG tests have been performed on compact tension, C(T), specimens extracted from weld regions of an ex-service 316H SS steam header component removed from one of the UK's AGR power plants to examine the influence of material degradation and inhomogeneity on the crack initiation and growth behaviour in near-weld regions. The starter cracks introduced into the C(T) specimens in this work were designed in such a way to replicate the reheat crack path in the actual steam header components by locating them in the regions close to and also further away from the fusion line. To investigate the specimen geometry effects on the CCG behaviour of the material in near-weld regions, an additional test was also performed on a single edge notched specimen in tension, SEN(T), and the results were compared to those of obtained from C(T) specimens.

It has been shown in previous studies that plastic pre-straining is introduced into engineering components during manufacturing processes such as bending, rolling and welding which influence the deformation and failure of high temperature welded components [14]–[16]. The change in the CCI and CCG behaviour in the pre-strained regions is expected to be due to the change in the mechanical properties and creep ductility of the pre-conditioned material [6]. Therefore, to account for the material pre-conditioning effects on the structural integrity assessment of high temperature welded steam headers, the results obtained from the current study are compared with those of available on the as-received (AR) material, heat affected zone (HAZ) and pre-strained material under compression (PC). The findings from this study have been discussed in terms of service exposure effects on microstructural deformation and macroscopic cracking behaviour of the aged steam headers to improve the current best practice in the structural integrity assessment of the these welded components.

2. Creep Deformation and Crack Growth Rules

2.1 Uniaxial Creep Deformation

According to the Norton's creep law [17], the stress dependency of the steady state creep strain rate, $\dot{\varepsilon}_s^c$ and average creep strain rate, $\dot{\varepsilon}_A^c$, can be expressed as

$$\dot{\varepsilon}_s^c = \dot{\varepsilon}_0 \left(\frac{\sigma}{\sigma_0} \right)^n = A_s \sigma^n \tag{1}$$

$$\dot{\varepsilon}_A^c = \dot{\varepsilon}_0 \left(\frac{\sigma}{\sigma_0} \right)^{n_A} = A_A \sigma^{n_A} \tag{2}$$

where σ is the applied stress, $\dot{\varepsilon}_0$ is the normalising strain rate, σ_0 is the normalising stress in power-law creep expression, n is the stress exponent in steady state creep strain rate power-law equation, n_A is the stress exponent in average creep strain rate power-law rule, and A_s and A_A are the Norton's power-law constants for steady state and average creep strain rates, respectively. The calculation of the minimum creep strain rate, average creep strain rate and a typical creep curve for 316H SS are schematically shown in Figure 1. As shown in this figure, the average creep strain rate $\dot{\varepsilon}_A^c$ can be simply calculated as the ratio of creep strain at failure (also known as creep ductility), ε_f, over rupture time, t_r.

Similarly, the correlation between the uniaxial rupture time, t_r, and applied stress level can be described using a power-law equation expressed as [18]

$$t_r = B_r \sigma^{-\nu_r} \tag{3}$$

where B_r is a material dependent constant and ν_r is a temperature dependent constant.

It has been shown in previous studies (e.g. [14] [15]) that the uniaxial creep deformation and failure behaviour of Type 316H SS can be described using the power-law equations given above.

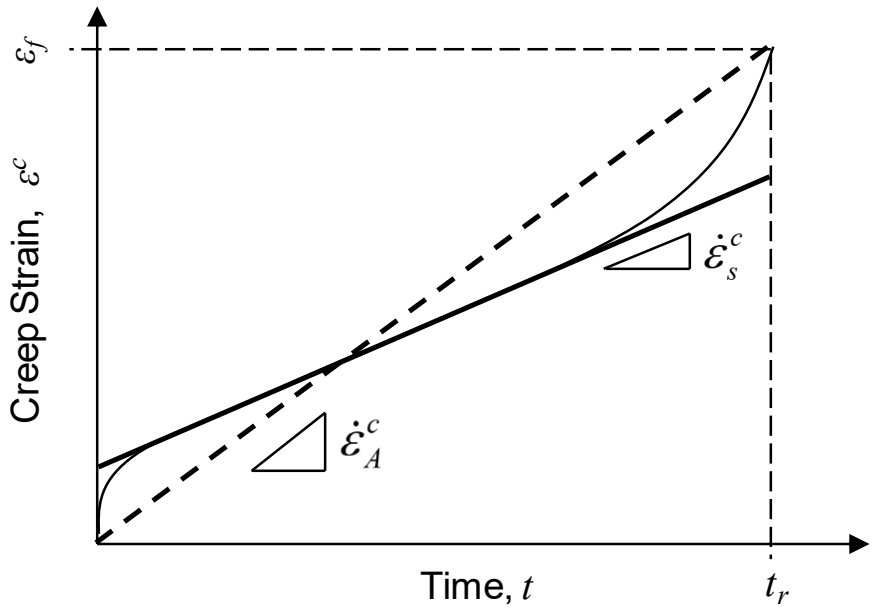

Figure 1: Schematic illustration of average creep strain rate, minimum creep strain rate and a typical creep curve for 316H steel

2.2 Creep Crack Initiation and Growth

For a power-law creeping material, the CCG rate, $\dot{a}$ (or da/dt), may be correlated with the C^* fracture mechanics parameter by

$$\dot{a} = DC^{*\phi} \tag{4}$$

where D and ϕ are the material constants and C^* values in CCG tests can be experimentally calculated by

$$C^* = \frac{P\dot{\Delta}}{B_n(W-a)}H\eta \tag{5}$$

where $\dot{\Delta}$ is the load line displacement rate, a is the crack length, P is applied load, W is specimen width, B_n is net thickness between the side grooves, and H and η are non-dimensional geometry dependent constants. For C(T) and SEN(T) specimen geometries, H can be described as $H = n/(n+1)$ where n is the Norton's law stress exponent. The η factor solutions for C(T) and SEN(T) specimen geometries can be found in [19]. It is worth noting that according to the recommendations in ASTM E1457 standard [19] the total load line displacement rate, as opposed to the creep displacement rate, can be employed in calculation of C^* parameter using equation (5). Moreover, although the procedures described in ASTM E1457 [19] are mainly applicable to homogenous materials, an extensive study was conducted in a previous work by the authors in [20] where the fracture mechanics solutions for inhomogeneous (cross-weld) specimens were examined and their dependency on the specimen geometry and crack length was investigated. The validity criteria for employing the C^* fracture mechanics parameter to describe the CCG behaviour of a material is described in the next section.

The initiation time, t_i, in CCG tests can be defined as the time taken for the crack to extend over a small distance after loading. This is typically of the order of 0.2-0.5 mm, depending on the sensitivity of the equipment used to detect the crack growth. The experimental definition of creep crack initiation time is regarded as $\Delta a = 0.2$ mm or $\Delta a = 0.5$ mm of crack extension, denoted as $t_{0.2}$ and $t_{0.5}$ [18]. The CCI time, t_i, may be experimentally correlated with the CCG rate $\dot{a}$ obtained from the experimental data and crack extension, Δa, by:

$$t_i = \frac{\Delta a}{\dot{a}} \tag{6}$$

2.3 C^* Validity Criteria

The validity criteria for correlating CCG rate with the C^* fracture mechanics parameter are specified in ASTM E1457 [19]. As described in ASTM E1457, the material is identified as 'creep-ductile' when the creep load line displacement rate constitutes at least half of the total load line displacement rate, $\dot{\Delta}^C / \dot{\Delta}^T \geq 0.5$. Subsequently, those data points obtained from the CCG tests which do not satisfy this criteria are considered invalid and cannot be correlated with the C^* fracture mechanics parameter.

The second validity criterion is to verify data points for which the time exceeds a transition time, t_T, which is defined as the maximum value of the term described in the following brackets:

$$t_T = Max\left[\frac{K^2}{E'(n+1)C^*(t)}\right] \tag{7}$$

where K is the stress intensity factor and E' is the effective Young's modulus where $E' = E$ for plane stress conditions and it is described as a function of elastic Young's modulus, E, and Poisson's ratio, ν, for plane strain conditions $E' = E/(1-\nu^2)$.

Additionally, the data points obtained prior to the time corresponding to 0.2 mm crack extension, $t_{0.2}$, where creep damage is building up to a steady state ahead of the crack tip should be excluded. Also, the data acquired after the accumulated load line displacement, Δ^{LLD}, greater than $0.05W$ are also considered invalid due to the additional bending moment as a result of the rotation of the arm.

Moreover, the R5 life assessment procedure [21] suggests an additional criterion for CCG rate correlation with C^*. According to the R5 guidelines, the non-dimensional crack velocity, λ, must be less than 0.5 for all valid times, where λ is defined as

$$\lambda = \frac{\dot{a}\sigma_{ref}^2}{EC^*} \tag{8}$$

where σ_{ref} is the reference stress, the solutions of which for different specimen geometries can be found in the literature (e.g. [22]).

2.4 NSW Creep Crack Growth Prediction Models

The NSW creep crack growth prediction model (called after Nikbin, Smith and Webster) provides an estimate of the CCG rate for a given value of C^* without the need to perform extensive number of experiments. [23]. According to the NSW model, the CCG rate $\dot{a}_{NSW}$ can be predicted using the uniaxial creep properties of the material using the following equation [24-25];

$$\dot{a}_{NSW} = \frac{(n+1)\dot{\varepsilon}_0}{\varepsilon_f^*}\left[\frac{C^*}{I_n\sigma_0\dot{\varepsilon}_0}\right]^{\frac{n}{n+1}} r_c^{\frac{1}{n+1}} = \frac{n+1}{\varepsilon_f^*}(Ar_c)^{\frac{1}{n+1}}\left[\frac{C^*}{I_n}\right]^{\frac{n}{n+1}} \tag{9}$$

where r_c is the size of the creep process zone and ε_f^* is the multiaxial creep ductility. According the NSW model, ε_f^* can be taken as the uniaxial creep ductility ε_f for plane stress conditions, and $\varepsilon_f/30$ for plane strain condition [25]. In the equation given above I_n is a dimensionless integration constant which depends on the Norton's law uniaxial creep stress exponent n and can be calculated using the following equations [18];

$$\begin{aligned} &\text{Plane stress: } I_n = 7.2\sqrt{0.12+\frac{1}{n}} - \frac{2.9}{n} \\ &\text{Plane strain: } I_n = 10.3\sqrt{0.13+\frac{1}{n}} - \frac{4.6}{n} \end{aligned} \tag{10}$$

It is worth noting that the CCG rate predictions using NSW model are often performed by employing the average creep strain rate exponent, n_A, in equations (9)-(10).

An approximate version of the NSW model (NSWA) was proposed in [26] where the CCG rate for a wide range of metallic materials can be predicted by;

$$\dot{a}_{NSWA} = \frac{3C^{*0.85}}{\varepsilon_f^*} \tag{11}$$

A modified version of the NSW model was derived in [27] in which the dependency of the creep strain on the crack tip angle θ, and the power-law creep stress component, n has been considered in CCG rate predictions. According to this mode, the crack growth is assumed to occur where the ratio of equivalent strain to the multiaxial failure strain, $\tilde{\bar{\varepsilon}}(\theta,n)/\varepsilon_f^*(\theta,n)$, reaches a maximum value, denoted as $\bar{h}_n$. The dependency of equivalent strain on crack tip angle, θ, follows from the crack tip strain rate fields (Riedel-Rice) where the creep strain rate is singular at the tip and varies with angle.

The CCG rate using NSW-MOD model is predicted by;

$$\dot{a}_{NSW-MOD} = \frac{(n+1)\dot{\varepsilon}_0}{\varepsilon_f^*}\left[\frac{C^*}{I_n\sigma_0\dot{\varepsilon}_0}\right]^{\frac{n}{n+1}} r_c^{\frac{1}{n+1}}\bar{h}_n \tag{12}$$

The value of multiaxial creep ductility, ε_f^* may be estimated from the uniaxial failure strain, using an appropriate void growth model such as Cocks and Ashby [28].

3. Specimen Preparation and Manufacture

In order to examine the CCG behaviour of 316H SS in near-weld regions, fracture mechanics specimens were extracted from an ex-service steam header provided by EDF Energy. The service exposed component was in service for 87,790 hours at operating temperature of around 550 °C, hence it was significantly aged under the operational loading conditions. Two C(T) specimens (denoted CT-1 and CT-NW-1) and one SEN(T) specimen (denoted SENT-1) were extracted from the weld region where a nozzle was attached to the thick-walled steam header using manual metal arc (MMA) welding. The key dimensions for the extracted fracture mechanics specimens including the width, W, the thickness, B, the net thickness between the side grooves, B_n, and the normalised initial crack length, a_0/W, are summarised in Table 1. As seen in Table 1, the C(T) specimens tested in the current study had the width of equal to or close to $W = 40$ mm. The initial normalised crack length was a_0/W= 0.5 in CT-1 and CT-NW-1. Also included in Table 1 are the C(T) specimen dimensions from other studies on PC and cross-weld (XW) specimens, the CCG results of which are compared with those of obtained from new specimens in the present study. The specimens which have been selected for comparison purposes are three C(T) extracted from the same 316H steam header with the material uniformly pre-compressed to 8% plastic strain at room temperature [15][16] and also two C(T) specimens with the starter crack located in the HAZ region extracted from a separate steam header of the same cast [23].

After extracting the C(T) and SEN(T) specimens, a starter crack was introduced into the fracture mechanics specimens using an EDM (electrical discharge machining) wire of 0.25 mm diameter. To examine near-weld CCG behaviour of the material in the ex-service steam header,

the C(T) specimens examined in this study were designed with two different crack orientations; (a) the starter crack located in the HAZ region near the fusion line, (b) the starter crack located in the base metal (BM), which is also known as the parent material, in near-weld region replicating the same angle of those reheat cracks observed in the ex-service header. One C(T) specimen (CT-NW-1) had the former orientation, which is schematically shown in Figure 2(a), while the latter was used for the design of the other C(T) sample (CT-1), which is schematically shown in Figure 2(b). Moreover, the starter crack in the SEN(T) specimen was located in the BM, similar to the orientation designed for CT-1. A schematic illustration of the starter crack location in the C(T) specimens with respect to the weld region is shown in Figure 2. The creep tests on all three samples examined in this study were performed at 550 °C.

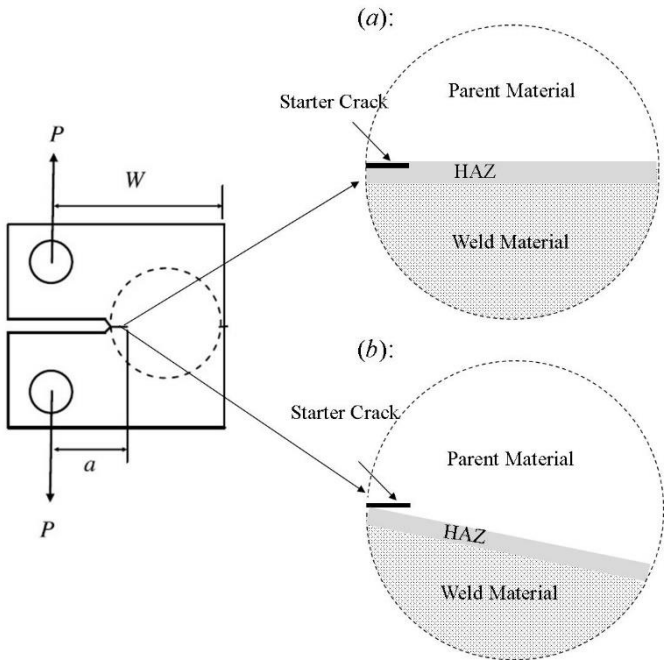

Figure 2: A schematic illustration of the starter crack position in C(T) specimens (a) crack growth along the HAZ region, (b) crack growth in parent material region

Table 1: Specimen geometry and dimensions

Test ID	Specimen Geometry	Crack Location	W (mm)	B (mm)	B_n (mm)	a_0/W
CT-1	C(T)	BM, near-weld	40	20	14.1	0.53
CT-NW-1	C(T)	Within HAZ	38	19	14.9	0.50
SENT-1	SEN(T)	BM, near-weld	25	12.5	12.5	0.30
8PC-A2[15]	C(T)	8% Pre-Compressed	50	25	17.5	0.35
8PC-A4[15]	C(T)	8% Pre-Compressed	50	25	17.5	0.50
8PC-D2[16]	C(T)	8% Pre-Compressed	50	25	20.0	0.50
XW-5[23]	C(T)	Within HAZ	50	25	20.0	0.51
XW-6[23]	C(T)	Within HAZ	50	25	20.0	0.52

4. Load Line Displacement and Crack Growth Results

CCG tests on CT-1, CT-NW-1 and SENT-1 specimens were performed at constants loads which are given in Table 2 and the results are compared with those of available in the literature on PC and XW specimens. The crack growth monitoring in these tests was performed using direct current potential drop (DCPD) technique and the output voltage measurements were calibrated post-testing following the procedure detailed in ASTM E1457 [19]. Moreover, the load line displacement (LLD) measurements on the fracture mechanics test specimens was carried out using linear variable differential transformers (LVDTs) which were located outside the furnace and attached to specimens using extension legs. A summary of the loading conditions and test results is presented in Table 2. The applied load level, P, stress intensity factor at the beginning of the test, $K(a_0)$, test duration, t_f, transition time, t_T, amount of crack extension, Δa, and the initiation times corresponding to 0.2 mm crack extension, $t_{0.2}$, and 0.5 mm crack extension, $t_{0.5}$, are summarised in Table 2.

Table 2: Summary of loading conditions and test results

Test ID	Load, P (kN)	$K(a_0)$ (MPa√m)	t_f (h)	Δa (mm)	t_T / t_f (%)	$t_{0.2} / t_T$ (%)	$t_{0.5} / t_T$ (%)
CT-1	10.3	32.5	1766	8.4	9.5	20.7	34.0
CT-NW-1	10.2	30.0	504	12.1	14.8	28.0	39.6
SENT-1	36.9	30.0	360	3.3	7.2	4.5	7.5
8PC-A2[15]	18.3	25.5	1303	8.5	5.0	0.7	2.9
8PC-A4[15]	12.1	25.0	194	9.4	3.9	4.8	54.5
8PC-D2[16]	12.9	25.0	357	11.9	5.5	5.0	33.6
XW-5[23]	15.6	31.1	718	11.8	7.8	37.0	-
XW-6[23]	14.5	29.9	736	17.3	3.8	4.5	-

4.1 Load Line Displacement Data

The variation of the total load line displacement, Δ, normalised by the specimen width, W, is plotted against time normalised by the test duration in Figure 3. Three types of specimens are illustrated in different colours; black for specimens tested in this study, red for PC specimens taken form [15][16] and finally blue for XW specimens with the initial crack located in the HAZ taken from [23]. As seen in this figure, the LLD variations were generally similar in all tests, except XW-5 and XW-6 which exhibited higher LLD values towards the end of the test. It can be observed in Figure 3 that the normalised load line displacement trends for CT-1 and SENT-1 are lower than other specimens towards the end of the tests. This can be associated with the fact that the crack in these two specimens was located in the BM near the weld region, therefore the LLD behaviour is more likely to be comparable with the AR specimens which are known to provide lower LLD trends compared to PC and HAZ specimens [6]. Note that

the slope of the normalised LLD trends towards the end of the tests depends on the test duration at which the test was stopped.

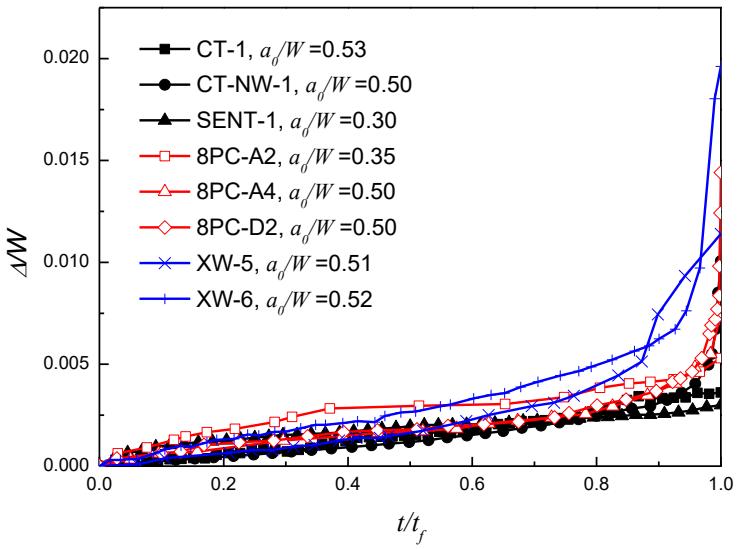

Figure 3: The load line displacement normalised by the specimen width plotted against the time normalised by the test duration for all specimens examined in this study

4.2 Crack Growth Data

In Figure 4, the crack extension, Δa, is plotted against the time normalised by the test duration for all the specimens considered in this study. Also included in this figure is a dashed line corresponding to 0.2 mm crack initiation time. As seen in Figure 4 all tests were stopped after crack extensions of much greater than 0.2 mm, and therefore there are enough data points available from these tests to characterise the CCG behaviour of the material using the C^* fracture mechanics parameter. Similar to LLD trends, the slope of the crack extension trends, particularly towards the end of the tests, is dependent on the points at which the test was stopped. Generally a smooth and slow crack growth trend towards the end of test was observed in CT-1 and SENT-1 specimens whilst large and rapid crack length extensions were observed in the XW, PC and CT-NW-1 specimens. Also seen in this figure is that the crack extension trend obtained from CT-NW-1 is consistent with XW-5 indicating that under similar loading conditions the crack growth behaviour is similar for the C(T) specimens with the starter crack located in the HAZ region. Finally seen in Figure 4 is that the obtained crack growth trend from 8PC-D2 C(T) specimen made of PC material is very similar to those of obtained from CT-NW-1 and XW-5 specimens. Comparing the test durations for these three tests in Table 2, it can be seen that under similar loading conditions, the test on the PC material was completed in much shorter time scales compared to the XW specimens (i.e. CT-NW-1 and XW-5). This suggests that the crack growth behaviour of the HAZ material can be estimated by performing short-term tests on the pre-strained material.

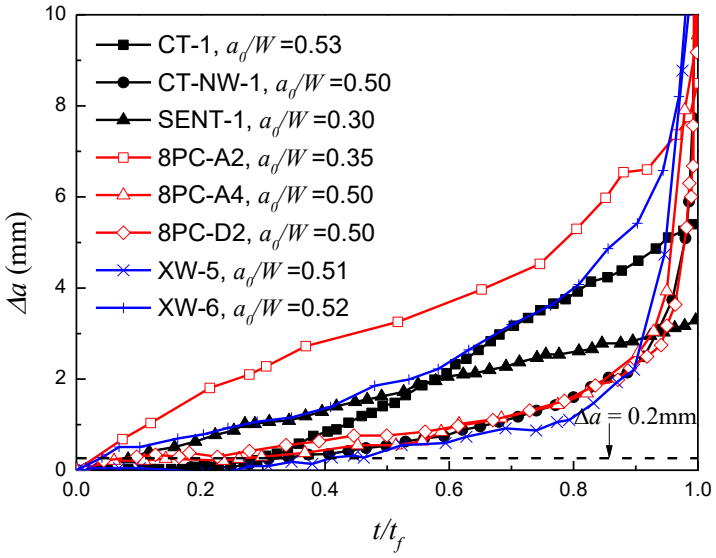

Figure 4: The crack length extension plotted against the time normalised by the test duration for all specimens examined in this study

4.3 Analysis of *C** Validity Criterion

The *C** validity criteria was applied on the data obtained from the specimen tested in this study and the results are summarised in Table 3. As seen in Table 3, λ and Δ^{LLD}/W criteria are satisfied by all specimens. It can be seen in Table 3 that in various tests the transition time t_T has occurred earlier or later than the initiation time $t_{0.2}$, hence both criteria were carefully applied to identify the valid data points in the analysis. The result of the *C** validity criteria is shown in Figure 5. As seen in this figure, the ratio of creep to total load line displacement rate is plotted against the time normalised by test duration. In this figure the valid data points which satisfy $t > t_{0.2}$ and $\dot{\Delta}^c / \dot{\Delta}^T \geq 0.5$ criteria are shown in solid black lines while the invalid data points are shaded in grey. As seen in Figure 5, a large proportion of data points obtained from different tests remain valid after consideration of the *C** validity criteria.

Table 3: *C** validity criterion according to ASTM E 1457 and R5 procedure

Test ID	t_f (h)	$t_{0.2}$ (h)	t_T (h)	Time for λ <0.5	Time for $\dot{\Delta}^c / \dot{\Delta}^T \geq 0.5$	Time for $\Delta^{LLD}/W \geq 0.05$
CT-1	1766	168	366	1766	1451	1766
CT-NW-1	504	75	141	504	458	504
SENT-1	360	26	16	360	360	360
8PC-A2[15]	1303	65	9	1303	670	1303
8PC-A4[15]	194	8	9	194	177	194
8PC-D2[16]	357	20	18	357	342	357
XW-5[23]	718	56	266	718	718	718
XW-6[23]	736	28	33	736	505	736

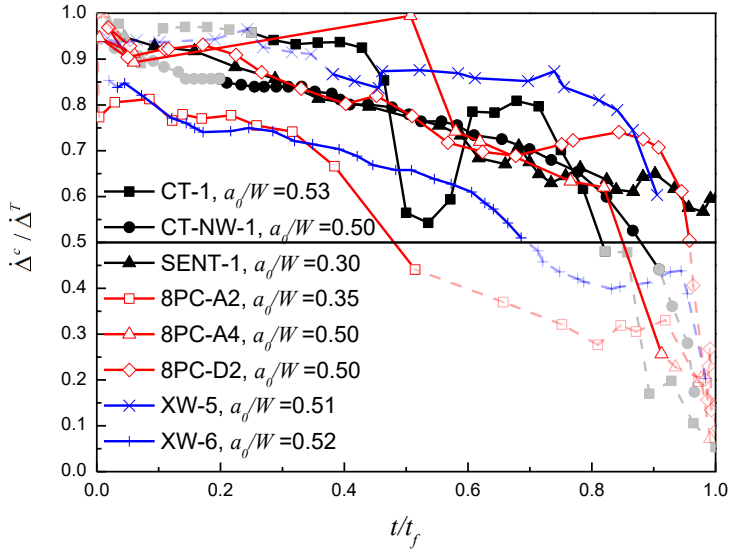

Figure 5: Analysis of C* validity criteria for the specimens examined in this study

5. Creep Crack Initiation and Growth Test Results

5.1 Creep Crack Growth Results

Assuming that steady state conditions are achieved after applying the C^* validity criteria, the CCG rates from the valid data points identified in Figure 5 have been correlated with the C^* fracture mechanics parameter and the results are shown in Figure 6. Also included in this figure are the experimental data band for the AR material state (i.e. BM) taken from [29]−[31] and shown in black dots, and also the data band for the C(T) HAZ specimens taken from [23] and shown in red dots. As seen in Figure 6, the CCG results from CT-NW-1 specimen fall within and towards the upper bound of the experimental data band for C(T) HAZ specimens, whereas the CCG results from CT-1 and SENT-1 samples fall within the experimental data band for the BM with the results from SENT-1 specimen showing a slightly lower trend compared to CT-1 specimen. This observation indicates that the crack growth behaviour in these two specimens is insensitive to the material inhomogeneity in near-weld region, hence the CCG behaviour of these two specimens is consistent with that of observed in specimens made of BM. Also seen in Figure 6 is that for a given value of C^* the CCG rate in the near-weld specimens with the crack tip in the BM is around an order of magnitude lower than the XW specimens (i.e. XW-5 and XW-6). As explained in [30], this is because of the loss of crack tip constraint due to plasticity and the increase in creep ductility in the BM specimens which result in a decrease in the CCG rate compared to XW specimens.

In Figure 6, the CCG data on 8% PC C(T) specimens taken from [15] [16] are compared with the HAZ data band and CT-NW-1 specimen. It can be seen that the CCG results from PC specimens fall upon CT-NW-1 data set with a similar slope in both material states suggesting that the CCG behaviour of the material within the HAZ region can be estimated with acceptable accuracy by performing tests on pre-strained material in much shorter timescales. These observations confirm the results presented in previous work [14] where it was shown that the CCG data in PC specimens may be used to estimate the behaviour of the HAZ material. Further seen in Figure 6 is that the slope (i.e. the power-law exponent ϕ in equation (4)) of near-weld specimens CCG data, which fall within the BM data band, is less than that in the HAZ and PC materials. According to the NSW model shown in equation (9), where the CCG rate is correlated with the C^* parameter using an exponent of $n/(n+1)$, this observation implies that the uniaxial power-law creep exponent, n, could be potentially lower in the near-weld BM compared to the HAZ and PC.

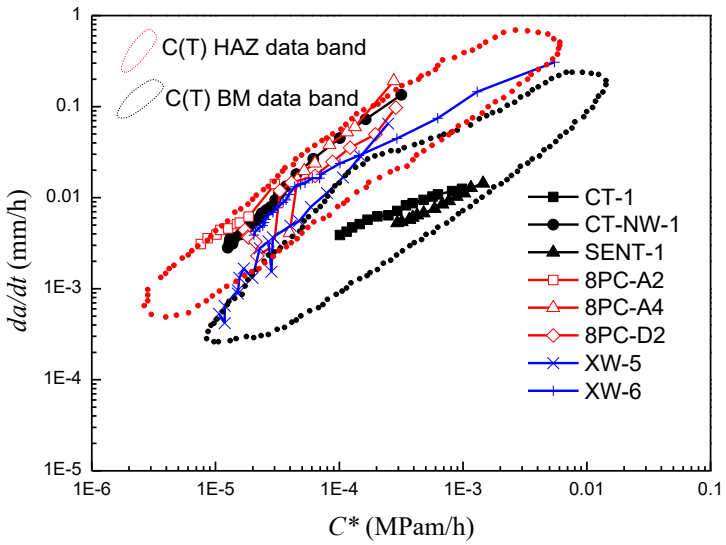

Figure 6: Creep crack growth rate correlation with the C^* fracture mechanics parameter for the specimens examined in this study

5.2 Creep Crack Growth Prediction using NSW Models

The experimental CCG data obtained from experiments were compared with the predictions made using the NSW models and the results are shown in Figure 7. The values of uniaxial creep properties employed in NSW models calculations were taken from [6][15][23] and are summarised in Table 4. The failure strain, ε_f used in all models was the uniaxial failure strain based on the reduction of area (ROA) which was measured before and after the tests. Also included in Table 4 are I_n and $\overline{h}_n$ values for plane strain (PE) conditions which are used in NSW models, and also the creep process zone size, which is often taken as the average grain size of the material.

Table 4: Uniaxial creep properties for 316H AR and HAZ materials at 550 °C employed in NSW models (taken from [6][15][23])

Type	A ($MPa^{-n}h^{-1}$)	n	ε_f (%)	r_c (mm)	I_n PE	$\overline{h}_n$ PE
AR	1.60×10^{-35}	11.9	21	0.05	4.42	11.58
HAZ	3.96×10^{-32}	10.9	10.32	0.05	4.42	11.58

The experimental CCG data examined in this study are compared with the prediction lines from NSW, NSWA and NSW-MOD models and the results are shown in Figure 7(a), Figure 7(b) and Figure 7(c), respectively. Considering the steady state linear region of the CCG data for the HAZ specimens it can be seen in Figure 7(a), (b) and (c) that the experimental data generally fall between plane stress (PS or $P\sigma$) and plane strain (PE or $P\varepsilon$) prediction lines using NSW, NSWA and NSW-MOD models. Also seen in Figure 7 is that the NSW and NSWA models provide conservative predictions of the CCG trends for plane strain conditions. However, NSW-MOD model provides a less conservative estimate of the CCG trends for plane strain conditions, and provides a good fit to the experimental HAZ data points. Further seen in Figure 7 is that the CCG data points from CT-1 and SENT-1 specimens fall close to but slightly below the NSW, NSWA and NSW-MOD plane stress prediction lines. Finally seen in Figure 7 (c) is that even though the NSW-MOD plane stress prediction line provides an approximate mean fit to the tested data to the BM, the CCG data points from CT-1 and SENT-1 specimens fall slightly below the prediction line and closer to the lower bound of the experimental data scatter band. In general, it can be observed in Figure 7 that the NSW-MOD plane stress and plane strain lines provide an excellent prediction of the CCG behaviour in the HAZ region while the predictions from all NSW models seem to be conservative for the BM.

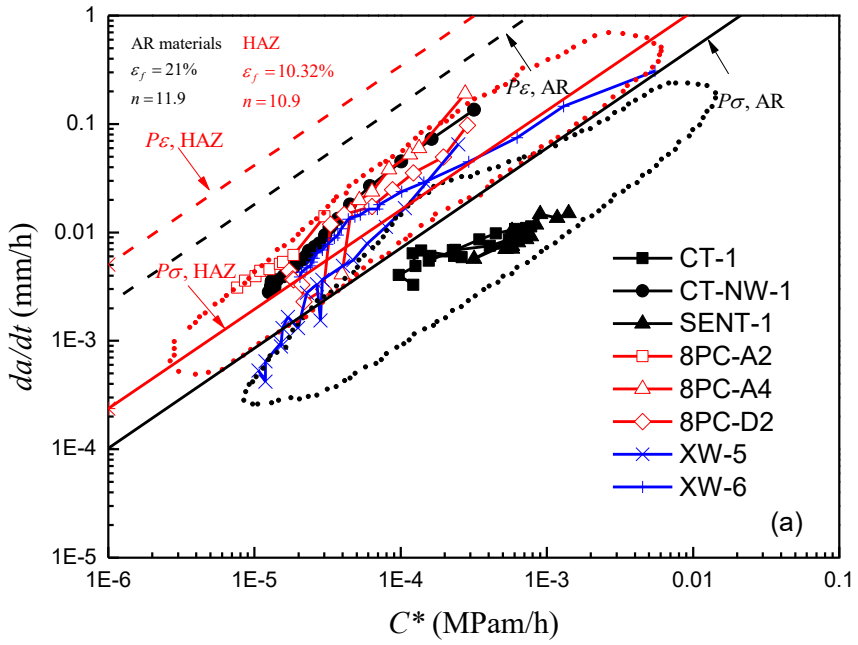

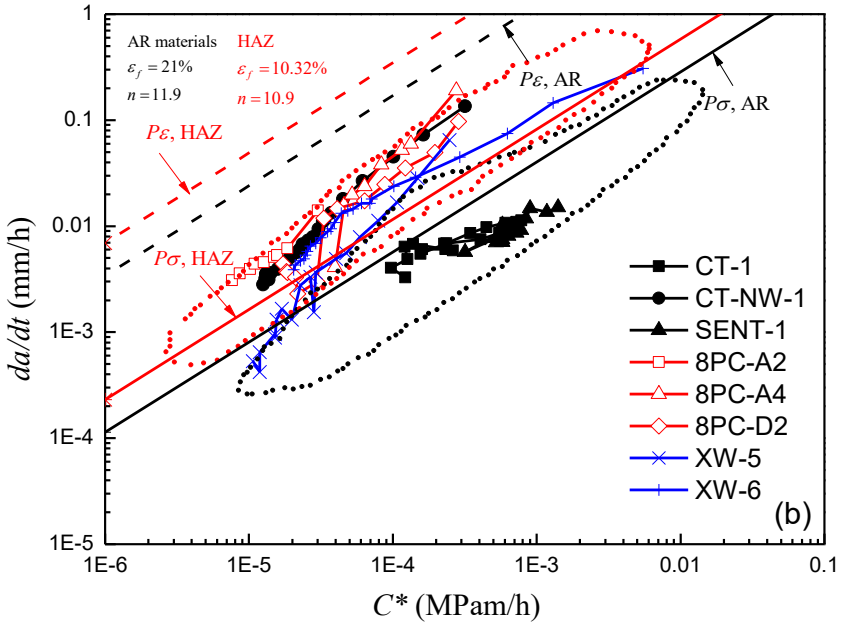

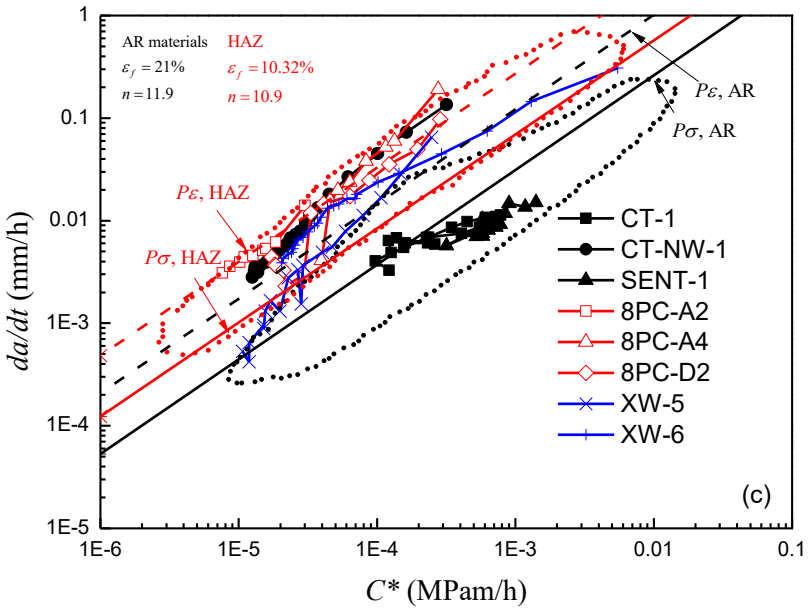

Figure 7: Comparison of the experimental data with CCG prediction results using (a) NSW, (b) NSWA, and (c) NSW-MOD models

5.3 Creep Crack Initiation Results

Assuming that steady state creep condition is achieved in the specimens examined in this study, the crack initiation times for crack extensions associated with 0.2 mm and 0.5 mm, denoted $t_{0.2}$ and $t_{0.5}$, obtained from the tests on CT-1, CT-NW-1 and SENT-1 specimens have been

correlated with the C^* fracture mechanics parameter and the results are shown in Figure 8(a) and Figure 8 (b), respectively. Also included in these figures are the experimental data from other tests on AR (i.e. BM), PC and HAZ specimens available in the literature [6][16][32]. In addition, the average CCI trends for the AR and HAZ material are calculated using Equation 6 and shown in Figure 8. The CCI trends for the AR and HAZ materials are shown in solid black and dashed red lines, respectively. As seen in Figure 8, although there is a large degree of scatter in $t_{0.2}$ and $t_{0.5}$ CCI data for the AR and HAZ specimens, the initiation times from CT-1 and SENT-1 specimens have been found to fall within the AR material scatter band whereas the CCI data point from CT-NW-1 specimen falls upon the HAZ CCI data band. Further tests are required to confirm the inferred CCI trends. Also seen in Figure 8(a) and Figure 8 (b) is that the CCI data obtained from the PC material are in good agreement with CT-NW-1 specimen and a conservative estimate of the CCI in XW specimens can be made in much shorter time scales by performing tests on PC material. Finally seen in Figure 8 is that for a given value of C^* the CCI in the HAZ material is around an order of magnitude shorter than the AR material. This may be associated with lower creep ductility in the HAZ material and also the presence of pre-existing defects in the weld region of the ex-service steam header from which the specimens were extracted.

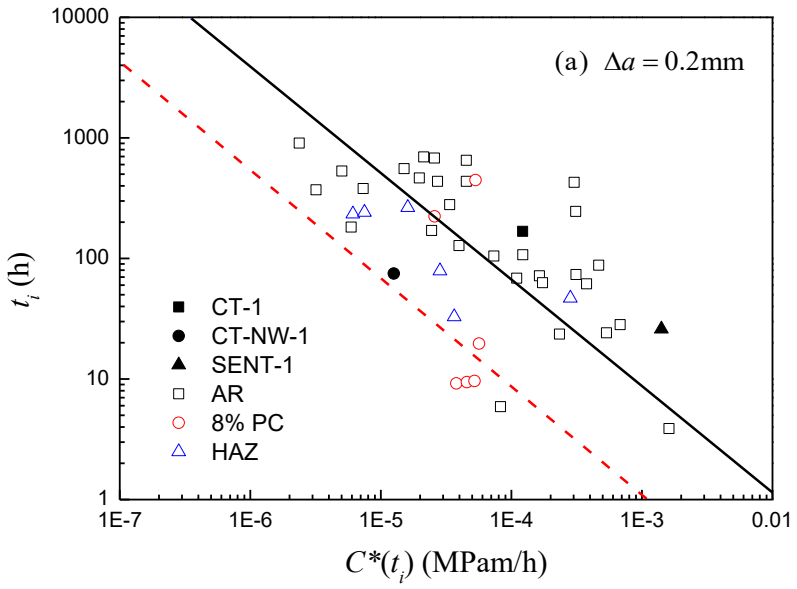

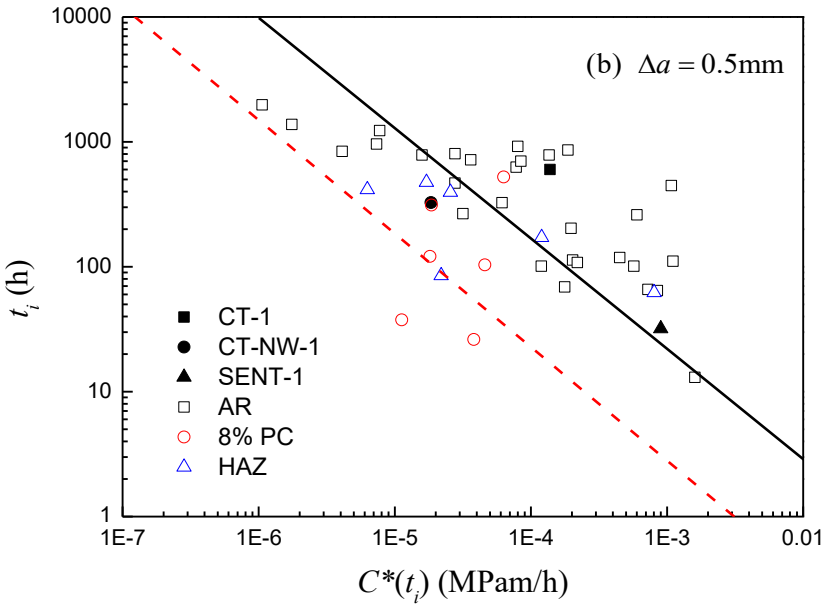

Figure 8: Initiation time correlation with the C^* parameter for (a) 0.2mm, (b) 0.5 mm crack extension

5.4 Crack Path Analysis

In order to study the cracking mode in the test specimens, slices were taken from each sample and analysed under the microscope. The cracking behaviour in all specimens was found similar, therefore only the result for SENT-1 is presented here for brevity. As seen in Figure 9, a slice of the SENT-1 specimen on a plane normal to the fracture surface was extracted, ground and polished to analyse the crack path using optical microscopy. It can be observed in this figure that in the vicinity of the starter crack, a continuous intergranular crack was initiated which grew for approximately 800 µm before branching started to occur in the specimen. Further seen in this figure is that ahead of the main crack, branched cracking morphology, micro cracks and creep cavities were observed with the intergranular micro-cracks oriented almost normal to the macroscopic crack path (i.e. hence parallel to the loading direction). As seen in this figure the voids mainly nucleate and grow on the grain boundaries and the well-developed cavities are then coalesced and form intergranular micro-cracks. Finally seen in Figure 9 is that although the crack path is showing a meandering behaviour above and below the specimen symmetry line, the macroscopic direction of the main crack is perpendicular to the loading direction. The observations from the optical microscopy analysis on 316H specimens are consistent with those of reported in the literature or other steels tested under creep loading conditions at high temperatures e.g. [33]-[35].

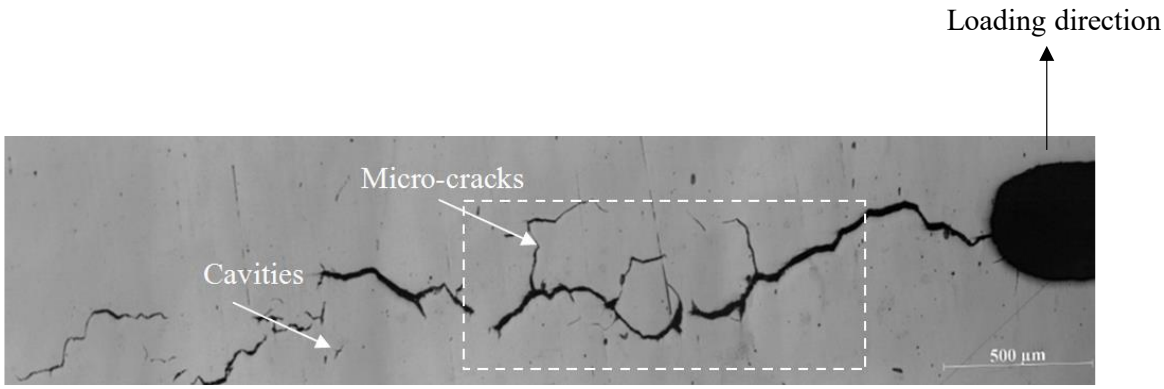

Figure 9: Optical microscopy of creep cracks in SENT-1 specimen

6. Conclusions

Creep crack initiation and growth tests were carried out on ex-service C(T) and SEN(T) specimens with the initial crack located within the HAZ region and in the BM in near-weld region to better understand the reheat cracking behaviour in those regions where weld residual stresses are present. The obtained CCI and CCG results from these tests were compared with those of available in the literature on BM, XW and PC materials. The key findings from the present study are summarised below:

1) When the cracks initiate in the BM within the near-weld region, the CCI and CCG behaviour is similar to the AR material. This implies that the welding procedure does not affect the creep crack behaviour on the surrounding material in the BM region.
2) The CCG behaviour in the HAZ and PC materials are similar, but their CCG rates are around an order of magnitude higher than the AR material.
3) The CCG behaviour of ex-service 316H material can be predicted using the the NSW models with the NSW-MOD model providing a less-conservative prediction of the CCG rate compared to NSW and NSWA models.
4) An inherent experimental scatter was observed in the CCI data obtained from AR, HAZ and PC specimens with the creep crack initiation time on average around an order of magnitude shorter in the HAZ material compared to the AR material.
5) The CCI and CCG behaviour of the HAZ material can be estimated with an excellent accuracy by performing short-term tests on uniformly pre-strained material.

7. References

[1] F. Vakili-Tahami and D. R. Hayhurst, “Failure of a welded pressure vessel due to creep: damage initiation, evolution and reheat cracking,” *Philos. Mag.*, vol. 87, no. 28, pp. 4383–4419, Aug. 2007.

[2] P. J. Holt, “Heysham I/Harlepool Superheater Weld S4: Revised Finite Element Residual Stress and Reheat Cracking Analysis,” British Energy Report, EPD/AGR/REP/0326/97, Issue 1, 1998

[3] R. P. Skelton, I. W. Goodall, G. A. Webster, and M. W. Spindler, “Factors affecting reheat cracking in the HAZ of austenitic steel weldments,” *Int. J. Press. Vessel. Pip.*, vol. 80, no. 7–8, pp. 441–451, Jul. 2003.

[4] D.J. Smith, P. J. Bouchard, and D. George, “Measurement and prediction of residual stresses in thick-section steel welds,” *J. Strain Anal. Eng. Des.*, vol. 35, pp. 287–305, 2000.

[5] D. R. Hayhurst, F. Vakili-Tahami and J. Q. Zhou, “Constitutive equations for time independent plasticity and creep of 316 stainless steel at 550 °C,” *Int. J. Press. Vessel. Pip.*, vol. 80, no. 2, pp. 97–109, Feb. 2003.

[6] A. Mehmanparast, C. M. Davies, D. W. Dean, and K. Nikbin, “Material pre-conditioning effects on the creep behaviour of 316H stainless steel,” *Int. J. Press. Vessel. Pip.*, vol. 108–109, no. 0, pp. 88–93, Aug. 2013.

[7] C. M. Davies, D. Hughes, R.C. Wimpory, D.W. Dean and K.M. Nikbin, “Measurements of Residual Stresses in 316 Stainless Steel Weldments,” in *Proceedings of the ASME 2010 Pressure Vessels&Piping Division/ K-PVP Conference*, July 18–22, Bellevue, USA, 2010 (Vol. 49255, pp. 1265-1273).

[8] L.Y. Chen, G.Z. Wang, J.P. Tan, F.Z. Xuan and S.T. Tu. “Effects of residual stress on creep damage and crack initiation in notched CT specimens of a Cr–Mo–V steel.” Engineering Fracture Mechanics, 97, pp.80-91, 2013.

[9] N.P. O’dowd, K.M. Nikbin and F.R. Biglari. “Creep crack initiation in a weld steel: effects of residual stress.” In ASME Pressure Vessels and Piping Conference (Vol. 4191, pp. 843-851, 2005).

[10] X.M. Song, G.Z. Wang, F.Z. Xuan and S.T. Tu. “Investigation of residual stress effects on creep crack initiation and growth using local out-of-plane compression.” Engineering Fracture Mechanics, 149, pp.45-57, 2015.

[11] M. Turski, A.H. Sherry, P. J. Bouchard and P.J. Withers. “Residual stress driven creep cracking in type 316 stainless steel.” Journal of neutron research, 12(1-3), pp.45-49, 2004.

[12] B. Chen, J.N. Hu, P.E.J. Flewitt, A.C.F. Cocks, R.A. Ainsworth, D.J. Smith, D.W. Dean and F. Scenini. “Effect of thermal ageing on creep and oxidation behaviour of Type 316H stainless steel.” Materials at High Temperatures, 32(6), pp.592-606, 2015.

[13] M.L. Zhu, D.Q. Wang and Xuan, F.Z. “Effect of long-term aging on microstructure and local behavior in the heat-affected zone of a Ni–Cr–Mo–V steel welded joint.” Materials characterization, 87, pp.45-61, 2014.

[14] C. M. Davies, D. W. Dean, A. Mehmanparast, and K. M. Nikbin, “Compressive pre-strain effects on the creep and crack growth behaviour of 316H stainless steel,” in *International Conference on Pressure Vessels and Piping*, July 18–22, Bellevue, USA, 2010 (Vol. 49255, pp. 323-330).

[15] A. Mehmanparast, C. M. Davies, D. W. Dean, and K. M. Nikbin, "The influence of pre-compression on the creep deformation and failure behaviour of Type 316H stainless steel," *Eng. Fract. Mech.*, vol. 110, no. 0, pp. 52–67, Sep. 2013.

[16] A. Mehmanparast, C.M. Davies, D.W. Dean and K. Nikbin, "Effects of plastic pre-straining level on the creep deformation, crack initiation and growth behaviour of 316H stainless steel." International journal of pressure vessels and piping, 141, pp.1-10, 2016.

[17] F.H. Norton, "The creep of steel at high temperatures." (No. 35). McGraw-Hill Book Company, Incorporated, 1929.

[18] G. Webster and R. A. Ainsworth, "High Temperature Component Life Assessment." Springer, 1994.

[19] "ASTM. E 1457-19: Standard test for measurement of creep crack growth times in metals," *Annu. B. ASTM Stand.*, vol. 3, no. 1, pp. 936–50, 2019.

[20] H. Zhou, F. Biglari, C.M. Davies, A. Mehmanparast and K.M. Nikbin. "Evaluation of fracture mechanics parameters for a range of weldment geometries with different mismatch ratios." *Eng. Fract. Mech.*, vol 124, pp.30-51, 2014.

[21] EDF Energy Nuclear Generation Ltd., "R5: Assessment Procedure for the High Temperature Response of Structures." Issue 3, 2003.

[22] T.L. Anderson. "Fracture mechanics: fundamentals and applications." CRC press, 2017.

[23] C. M. Davies, D. W. Dean, K. M. Nikbin, and N. P. O'Dowd, "Interpretation of creep crack initiation and growth data for weldments," *Eng. Fract. Mech.*, vol. 74, no. 6, pp. 882–897, Apr. 2007.

[24] K. Nikbin, D.J. Smith and G.A. Webster. "Influence of creep ductility and state of stress on creep crack growth." Advances in life prediction methods at elevated temperatures, pp.249-258, 1983.

[25] K. Nikbin, D.J. Smith and G.A. Webster, "An engineering approach to the prediction of creep crack growth," Journal of Engineering Materials and Technology, 108, pp. 186-191, 1986.

[26] K. Nikbin, D.J. Smith and G.A. Webster, "Prediction of creep crack growth from uniaxial creep data." Proceedings of the Royal Society of London. A. Mathematical and Physical Sciences, 396(1810), pp.183-197, 1984.

[27] M. Yatomi, N.P. O'Dowd, K. Nikbin and G.A. Webster, "Theoretical and numerical modelling of creep crack growth in a carbon–manganese steel." Engineering Fracture Mechanics, 73(9), pp.1158-1175, 2006.

[28] A.C.F. Cocks and M.F. Ashby, "Intergranular fracture during power-law creep under multiaxial stresses." Metal science, 14(8-9), pp.395-402, 1980.

[29] D. W. Dean and D. N. Gladwin, "Creep crack growth behaviour of Type 316H steels and proposed modifications to standard testing and analysis methods," *Int. J. Press. Vessel. Pip.*, vol. 84, no. 6, pp. 378–395, Jun. 2007.

[30] A. Mehmanparast, C.M. Davies, G.A. Webster and K. Nikbin, "Creep crack growth rate predictions in 316H steel using stress dependent creep ductility." Materials at High Temperatures, 31(1), pp.84-94, 2014.

[31] A. Mehmanparast, “Prediction of creep crack growth behaviour in 316H stainless steel for a range of specimen geometries.” International Journal of Pressure Vessels and Piping, 120, pp.55-65, 2014.

[32] H. Quintero and A. Mehmanparast, “Prediction of creep crack initiation behaviour in 316H stainless steel using stress dependent creep ductility.” International Journal of Solids and Structures, 97, pp.101-115, 2016.

[33] J.-F. Wen and S.-T. Tu, “A multiaxial creep-damage model for creep crack growth considering cavity growth and microcrack interaction,” *Eng. Fract. Mech.*, vol. 123, no. 0, pp. 197–210, Jun. 2014.

[34] A. Mehmanparast, C.M. Davies, D.W. Dean and K.M. Nikbin, “Plastic pre-compression and creep damage effects on the fracture toughness behaviour of Type 316H stainless steel.” *Eng. Fract. Mech*, vol. 131, pp.26-37, 2014.

[35] A. Mehmanparast and C.M. Davies, “The influence of inelastic pre-straining on fracture toughness behaviour of Type 316H stainless steel.” *Eng. Fract. Mech*, vol. 188, pp.112-125, 2018.